Electronic Supplementary Material (ESI) for ChemComm.

Zn(002)-Preferred and pH-Buffering Triethanolamine as Electrolyte Additive for Dendrite-Free Zn Anodes

Wenjing Ge,[a] Huili Peng,[a,b] Jingjing Dong,[a] Gulian Wang,[a] Lifeng Cui,[c] Wei Sun,[c] Xiaojian Ma,[a] and Jian Yang*[a]

[a]Key Laboratory of Colloid and Interface Chemistry, Ministry of Education, School of Chemistry and Chemical Engineering, Shandong University, Jinan 250100, China. E-mail: yangjian@sdu.edu.cn
[b]School of Chemistry and Chemical Engineering, Linyi University, Linyi 276000, P. R. China.
[c]Shandong Hualu-Hengsheng Chemical Co. Ltd., Dezhou 253024, P. R. China.

Experimental Section

Materials

Commercial Zn foils (purity 99.99%) were purchased from Cyber and Cu foils (purity 99%) were purchased from Guangdong Canrd New Energy Technology, which were washed with deionized water and ethanol for several times before use. $ZnSO_4 \cdot 7H_2O$ (purity 99.5%), Triethanolamine (TEOA, purity 99.0%), glycerol (GLY, purity 99.0%), H_2SO_4 (purity 98.0%) and isopropanol (purity 99.7%) were purchased from Sinopharm Chemical Reagent Co. Ltd. Zinc trifluoromethanesulfonate ($Zn(OTf)_2$, purity 98%), polyaniline (PANI, purity 98%), triisopropanolamine (TIPA, purity 95%) and Deuterium oxide (D_2O, purity 99.9%) were obtained from Macklin. Triethylamine (TEA, purity 99.5%), N-Methyl pyrrolidinone (NMP, 99.0%) and polytetrafluoroethylene (PTFE, purity 60 wt%) were obtained from Aladdin. Zinc chloride ($ZnCl_2$, purity 98%) and Zinc di[bis(trifluoromethylsulfonyl)imide] ($Zn(TFSI)_2$) were obtained from Sigma Aldrich. The Zn foils were cut into circle pieces with a diameter of 12 mm and the Cu foils were cut into circle pieces with a diameter of 14 mm before use. All of the reagents were directly used without further purification.

Electrolytes

2 M $ZnSO_4$: Used analytical balance (Mettler Toledo, ME104E/02, Shanghai, China) to weigh 57.5120 g $ZnSO_4 \cdot 7H_2O$ (0.2 mol) into a 100 mL volumetric bottle, added distilled water to the scale line, and shook well.

2 M $ZnSO_4$-x M TEOA: Used analytical balance to weigh 57.5120 g $ZnSO_4 \cdot 7H_2O$ (0.2 mol) into a 100 mL volumetric bottle, and added 1.4919 g (0.01 mol), 7.4595 g (0.05 mol), 14.9190 g (0.1 mol) TEOA to it, then added appropriate amount of water to the volumetric bottle. 2 M H_2SO_4 was dispersed into the solution until the white precipitate disappeared completely, finally added distilled water and evenly mixed to the scale line. The preparation of $ZnSO_4$-TEA, $ZnSO_4$-GLY, $ZnSO_4$-TIPA, $Zn(OTf)_2$, $ZnCl_2$, $Zn(TFSI)_2$, $Zn(OTf)_2$-TEOA, $ZnCl_2$-TEOA, $Zn(TFSI)_2$-TEOA refer to the preceding method.

Materials Characterization

X-ray diffractometer (XRD) patterns were recorded by an XRD diffractometer (Rigaku, SmartLab 9KW, Japan), with mono-chromatic Cu kα as the radiation source (λ = 1.5418 Å). Polar figures were obtained by a high-resolution diffractometer (Xpert pro mrd3, Panaco, Netherlands).Scanning electron microscope (SEM) images and X-ray energy dispersive spectra (EDS) were obtained by a field emission scanning electron microscope (FESEM, Zeiss Gemini 300, Germany) coupled with an X-ray energy dispersive spectrometer (Oxford Instruments INCAx, England). Atomic force microscopy (AFM) images were measured on a scanning probe microscope (Bioscope Resolve, Brucker, Germany). The in-situ optical images were obtained from an optical microscope (YM520R, Suzhou YUESHI, China). X-ray photoelectron spectra (XPS) were achieved from a Thermo Fisher Scientific Model K-Alpha spectrometer equipped with Al Kα radiation (1486.6 eV). The XPS spectra were calibrated with the binding energy of C 1s (C sp^2) as 284.8 eV. Fourier-transformed infrared spectra (FT-IR) were measured on an IR spectrometer (Bruker Tensor-II FT-IR, Germany). ^1H NMR nuclear magnetic resonance spectra were acquired on an AVANCE III HD 400 spectrometer (AVANCE NEO, Brucker, Germany) and D_2O was used as the solvent. Raman spectra were characterized using an excitation of 532 nm at room temperature on a micro-Raman spectrometer (Gamry, Refence 3000+iRaman, USA). The viscosity of electrolytes was obtained from the temperature test viscometer (MSK-SFM-VT8s, Shenzhen KeJingStar, China). The conductivity of the electrolytes was obtained by the conductivity meter (DDSJ-308F, Shanghai LEICI, China). The pH was measured via pH meter (FE28, Shanghai Mettler Toledo, China) and pH planar electrode (LabSen 371, Shanghai Sanxin, China).

Electrochemical Measurements

For room temperature testing, the electrochemical performances of Zn anodes were evaluated in CR2025-type coin (Canrd Co., Ltd.) cells. The non-woven fabrics (WIP-0609 SERIES) were used as separator. The electrolytes were $ZnSO_4$ and $ZnSO_4$-TEOA. In the half cells, the Zn||Zn cells were galvanostatically tested at different current

densities and areal capacities by using the LAND CT-2001A battery tester. The pouch cells of Zn||Zn with areas of 20 cm^2 (4 cm × 5 cm) were assembled in air using three layers of non-woven fabrics as the separator to observe *in-situ* of the pH changes during charging process under 10 mA cm^{-2} and 10 mAh cm^{-2}. The Zn||Cu cells were tested at a current density of 2 mA cm^{-2}. In each cycle, metallic Zn was deposited onto Cu substrate during discharging then the cells were charged to the cutoff voltage of 0.5 V (vs. Zn^{2+}/Zn) at the same current.

In the full cells, PANI was used as the cathode material. It was prepared by mixing 70 wt% of PANI, 10 wt% carbon nanotubes (CNTs, XF Nano.), 10 wt% acetylene black (AB, DoDoChem) and 10 wt% polyvinylidene fluoride (PVdF, DoDoChem) in NMP. Then, the obtained slurry was spread on carbon paper (Jinglong Special Carbon Tech.) and dried under vacuum at 60 °C for 12 h. The mass loading of PANI in the cathode was about ~1 mg cm^{-2}. After that, the cathode was punched into small discs with a diameter of 10 mm. These discs as cathode were assembled with Zn foil as anode (thickness: 30 μm, diameter: 12 mm), $ZnSO_4$ or $ZnSO_4$-TEOA as electrolytes and two layers of non-woven fabrics as separator into coin cells. Here, the amount of Zn in full cell is extremely excess in view of the capacity. Thus, the thick cathode was prepared to approach the practical applications. A paste for the thick cathode was developed by mixing 60 wt% of PANI, 15 wt% of acetylene black, 15 wt% CNTs and 10 wt% of PTFE in isopropanol. Then, the paste was rolled into a freestanding film. After being dried in an oven at 80 °C, the film was punched into small discs with a diameter of 10 mm and then pressed onto the stainless-steel mesh (diameter: 12 mm) for electrochemical testing. The mass loading of PANI was ~10 mg cm^{-2} and the thick cathode was coupled with Zn foil (30 μm). In addition, the full cells were tested under harsh conditions (N:P ratio =4.2, the dosage of electrolyte is 44.6 μL mAh^{-1}). The pouch cells of Zn||PANI with areas of 49.5 cm^2 (5.5 cm × 9 cm) were assembled in air using three layers of non-woven fabrics as separator. Galvanostatic charge/discharge (GCD) profiles were obtained on a battery cycler (LAND CT-2001A, China). All Zn||PANI cells were tested over the range of 0.4~1.65 V at the room temperature with $ZnSO_4$ or $ZnSO_4$-TEOA.

The cyclic voltammetry (CV), linear sweep voltammetry (LSV), linear polarization (LP) curves were obtained on an electrochemical workstation (CHI 760E, China) at room temperature. To be specific, the CV tests were conducted at a scan rate of 1 mV s^{-1} in a two-electrode configuration, in which Zn foil was anode, and PANI coating on carbon cloth was cathode. The LSV measurement was carried out at a scan rate of 1 mV s^{-1} in a two-electrode configuration, Zn was anode, stainless steel was cathode. The LP curve was tested at a scan rate of 1 mV s^{-1} in a three-electrode configuration where Zn foil, Pt foil, Ag/AgCl was employed as working, counter and reference electrode, respectively. Chronoamperometry (CA) curves were measured by using an electrochemical workstation (Autolab PGSTAT 302N, Switzerland). More specifically, CA curves of Zn||Zn cells in $ZnSO_4$ or $ZnSO_4$-TEOA were tested at a constant potential of -200 mV.

The activation energy (Ea) of the desolvation process of hydrated Zn^{2+} in $ZnSO_4$ and $ZnSO_4$-TEOA were estimated by the law of Arrhenius equation.

$$\frac{1}{R_{ct}} = A\ exp\ (-\frac{E_a}{RT})$$

Where R_{ct} is the interfacial resistance, A is the frequency factor, R is the gas constant, and T is the absolute temperature.

The data about depth of discharge (DOD) were acquired by the equations:

$$DOD_{(\%)} = \frac{C_{actual,\ area}}{C_{theoretical,\ area}} \times 100\% = \frac{C_{actual,\ area}}{l \times \rho \times C_{theoretical,\ mass}} \times 100\%$$

Where $C_{actual,\ area}$ (mAh cm^{-2}) is the actual areal capacity during the plating/stripping of Zn, $C_{theoretical,\ area}$ (mAh cm^{-2}) is the theoretical areal capacity of Zn foils, $C_{theoretical,\ mass}$ (mAh g^{-1}) is the theoretical mass capacity of Zn, l (cm) and ρ (g cm^{-3}) are the thickness and density of Zn foils, respectively. For example,

$$DOD_{(46\%)} = \frac{8\ mAh\ cm^{-2}}{0.003\ cm \times 7.14\ g\ cm^{-3} \times 820\ mAh\ g^{-1}} \times 100\% \approx 46\%$$

Calculate method of adsorption energy

The optimized structures and the adsorption energies were calculated at the DFT level as implemented in the Vienna Ab initio Simulation Package (VASP),[1] using a planewave basis set with an energy cutoff of 450 eV, the projector augmented wave (PAW) potentials, and the generalized gradient approximation (GGA) parametrized by Perdew, Burke, and Ernzerhof (PBE) for the exchange and correction interactions.[2, 3] The Brillouin zone was sampled by 2 × 1× 1 *k*-points, and the convergence criteria for residual force and energy were set to 0.05 eV $Å^{-1}$ and 10^{-4} eV, respectively. A vacuum space of 15 Å was added to the *c* direction to avoid interactions between periodic images.

The binding energy of Zn adsorbed on TEOA(O), H_2O and adsorption energy of TEOA and H_2O adsorbed on Zn (x), [x= (002), (100), (101)] are defined as:

$$\triangle E = E_{Zn/TEOA(O)} - E_{Zn} - E_{TEOA(O)}$$

$$\triangle E = E_{Zn/H_2O} - E_{Zn} - E_{H_2O}$$

$$\triangle E = E_{TEOA/Zn(x)} - E_{TEOA} - E_{Zn(x)}$$

$$\triangle E = E_{H_2O/Zn(002)} - E_{H_2O} - E_{Zn(002)}$$

where $E_{Zn/TEOA(O)}$, E_{Zn}, $E_{TEOA(O)}$, E_{Zn/H_2O}, E_{H_2O}, $E_{TEOA/Zn(x)}$, $E_{(TEOA)}$, $E_{Zn(x)}$, $E_{H_2O/Zn(002)}$ and $E_{Zn(002)}$ represent the total energy of Zn/TEOA(O), Zn, TEOA(O), Zn/H_2O, H_2O molecule, TEOA/Zn(x), TEOA molecule, Zn(x), H_2O/Zn(002) and Zn(002).

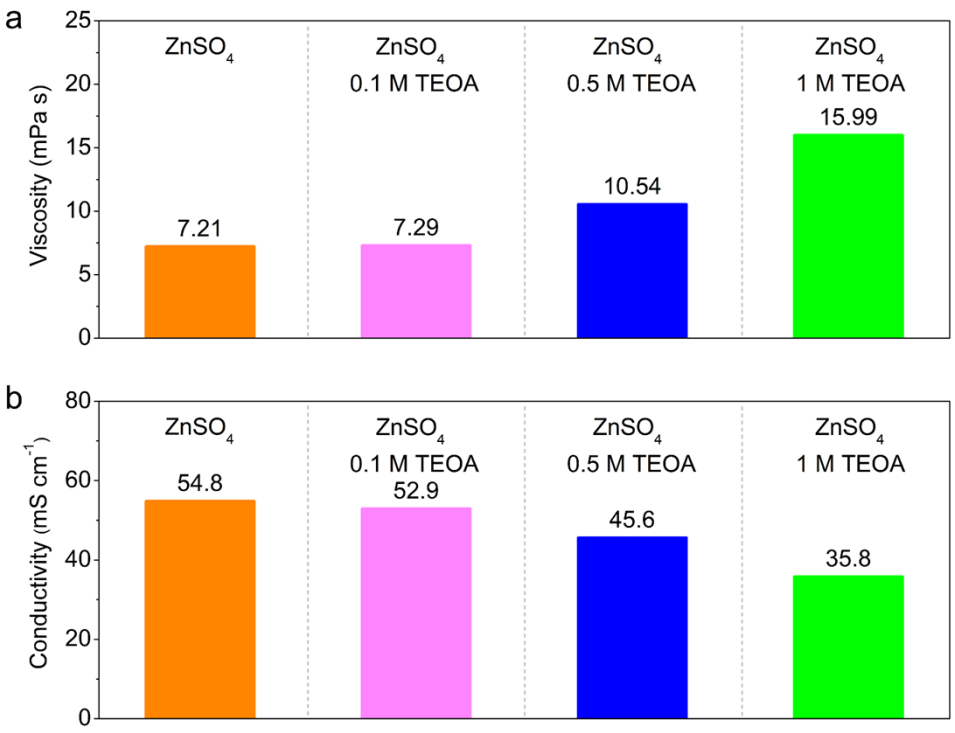

Fig. S1. Viscosity (a) and ion conductivity (b) of $ZnSO_4$ and $ZnSO_4$-x M TEOA (x=0.1, 0.5 and 1).

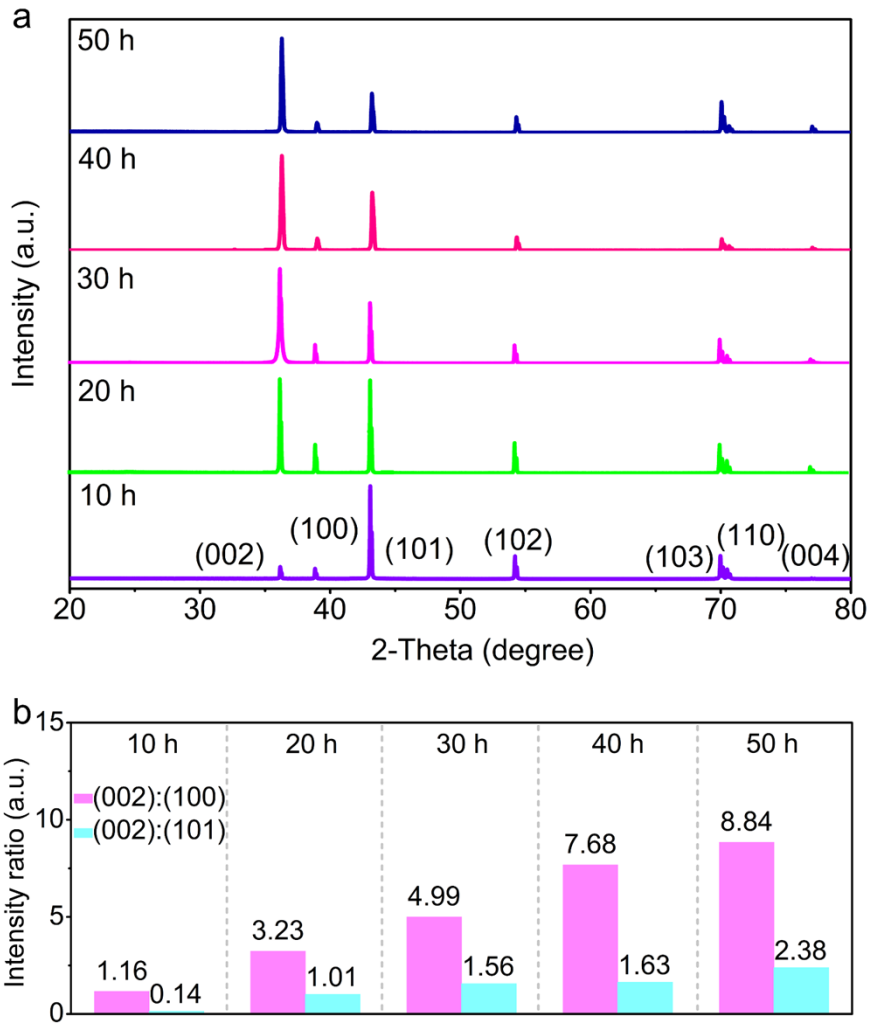

Fig. S2. (a) XRD patterns and (b) the peak intensity ratio of Zn(002)/Zn(100) and Zn(002)/Zn(101) in $ZnSO_4$-TEOA after different cycling times at 2 mA cm^{-2} and 1 mAh cm^{-2}.

The relatively diffraction intensity of Zn(002) facet gradually increases with the increase of the cycling times. The results well demonstrate the preferential growth of Zn(002) during cycles.

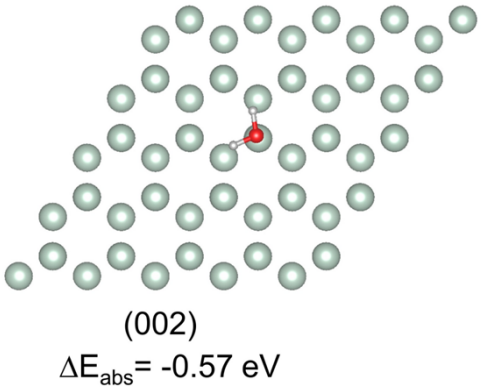

Fig. S3. The adsorption energy of H_2O adsorbed on Zn(002) facet.

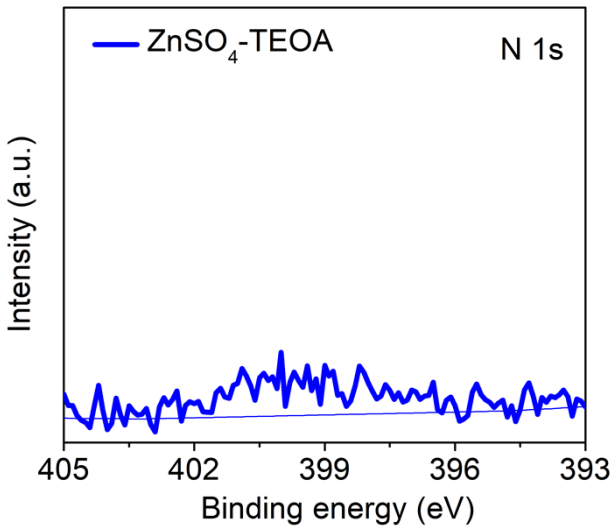

Fig. S4. N 1s spectrum of Zn foils after 50 cycles in $ZnSO_4$-TEOA at 2 mA cm^{-2} and 1 mAh cm^{-2}.

XPS is performed on the Zn anode to verify the stability of TEOA during the cell cycles. TEOA contain the characteristic N-element and 0.5 M high-concentration of TEOA is added to 2 M $ZnSO_4$. However, the ratio of N-signal to the noise signal on the surface of Zn foil in $ZnSO_4$-TEOA is very low, proving that TEOA in the electrolyte does not decompose. A very small bump of N-signal may be caused by the exposure of the electrode to the air.

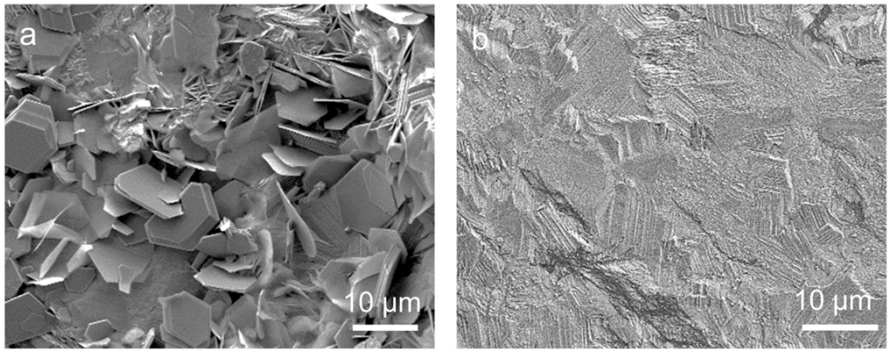

Fig. S5. SEM images of the Zn foil after 200 cycles at 2 mA cm^{-2} and 1 mAh cm^{-2} in different electrolytes, (a) pure electrolyte ($ZnSO_4$), (b) modified electrolyte ($ZnSO_4$-TEOA).

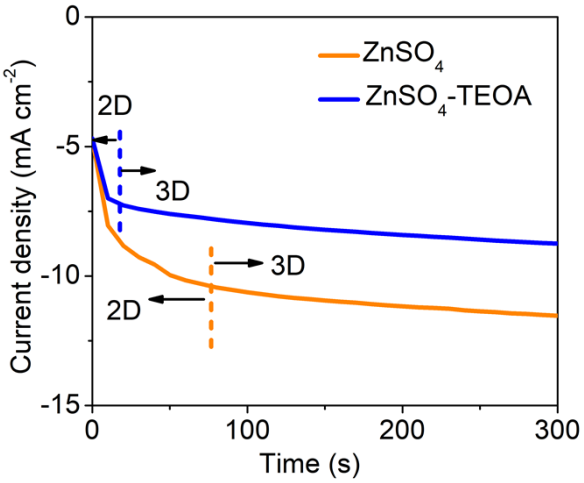

Fig. S6. CA curves of Zn||Zn cells in different electrolytes at the overpotential of -200 mV.

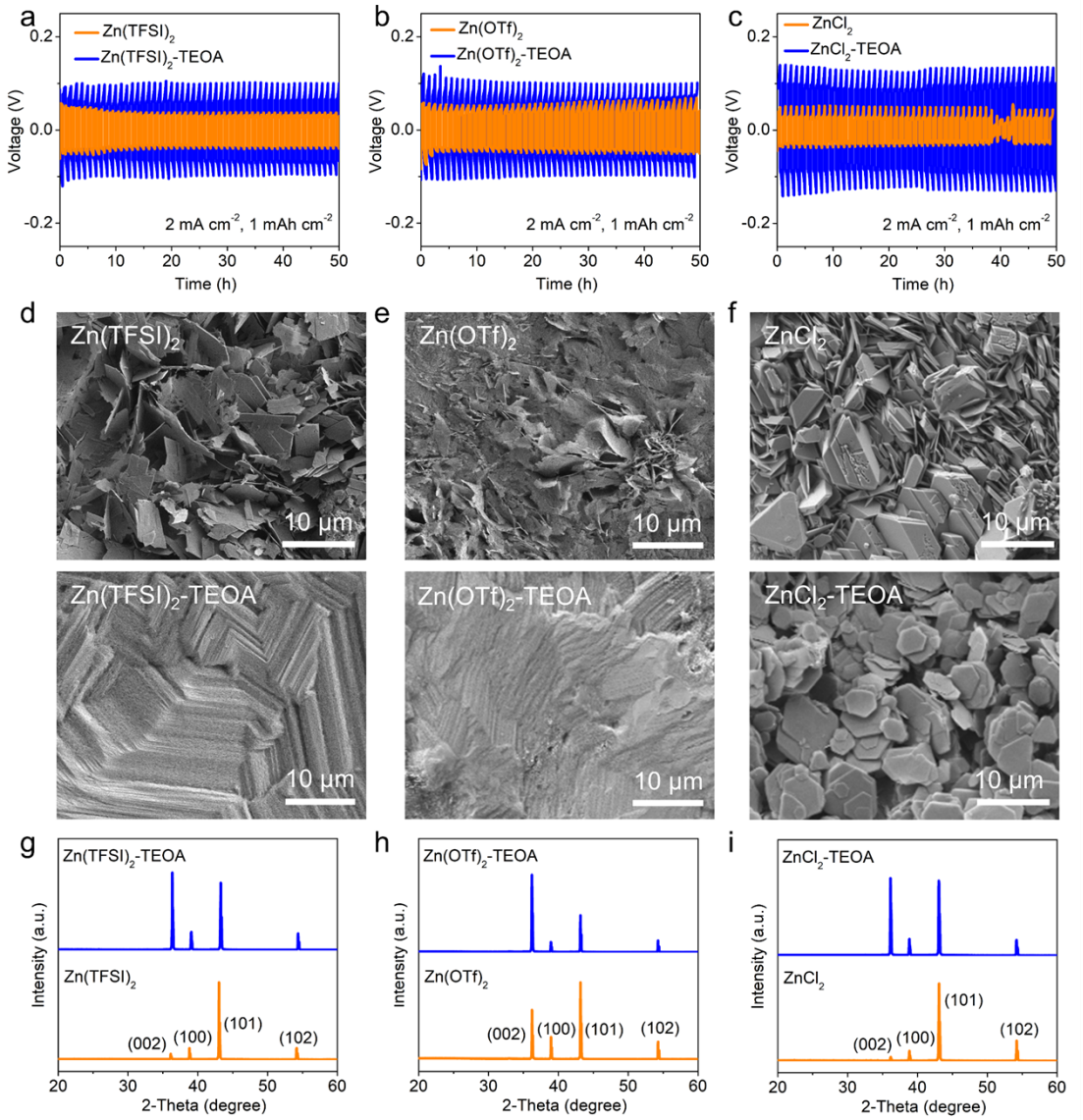

Fig. S7. (a-c) The polarization of Zn||Zn cells in different electrolytes system (a for $TFSI^-$, b for OTf^- and c for Cl^-) at 2 mA cm^{-2} and 1 mAh cm^{-2}; (d-f) SEM images of Zn foils after 50 cycles in different electrolytes; XRD patterns of Zn foils after 50 cycles in different electrolyte systems at 2 mA cm^{-2} and 1 mAh cm^{-2}, g for $TFSI^-$, h for OTf^- and i for Cl^-.

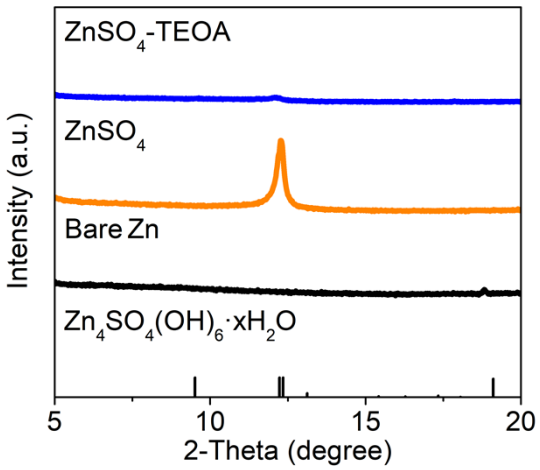

Fig. S8. XRD patterns of the Zn foils before and after 200 cycles in symmetric cells at 2 mA cm^{-2} and 1 mAh cm^{-2} in different electrolytes.

It is noted that the strong diffraction of $Zn_4SO_4(OH)_6 \cdot xH_2O$ (ZHS) at 12° appears in the XRD pattern of the Zn foil cycled in the pure electrolyte ($ZnSO_4$). On the contrary, it almost disappears in the case using TEOA as the electrolyte additive. This difference confirms the inhibition of TEOA on the formation of ZHS.

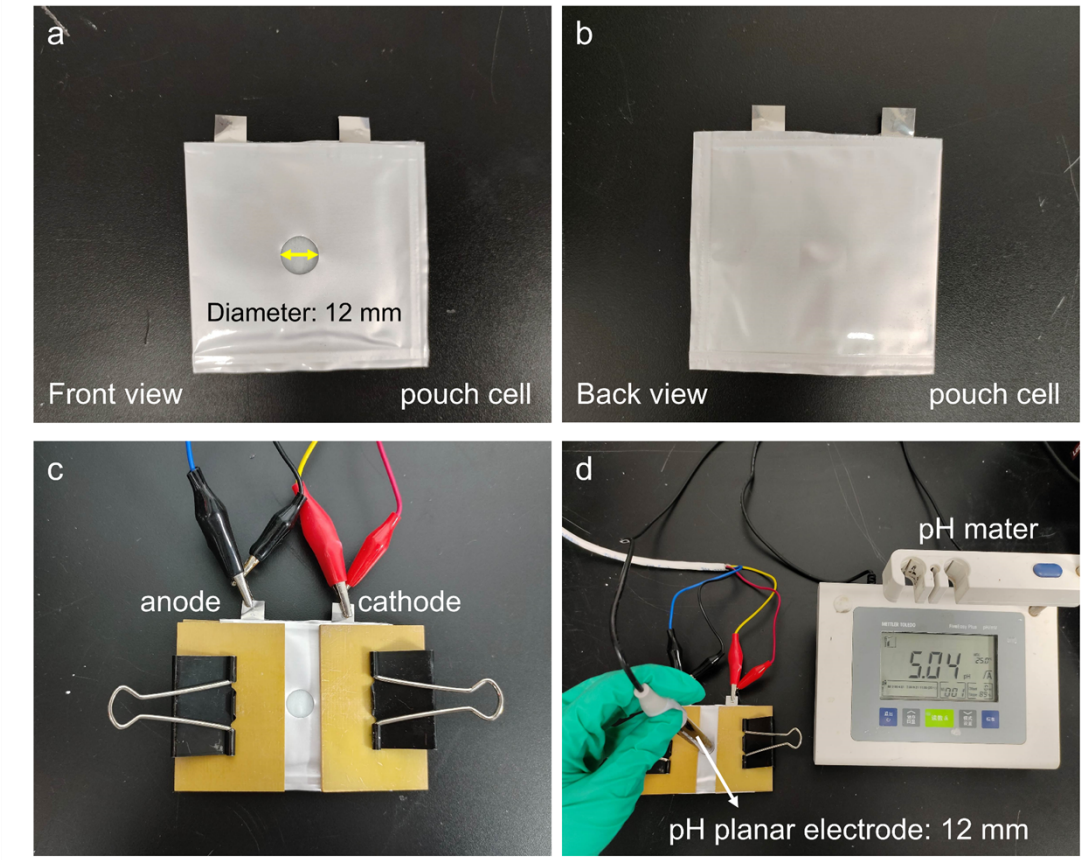

Fig. S9. (a, b) Pouch cells using the punched package and Zn foil; (c, d) Experimental set-up for pH detection near the Zn anodes.

Firstly, a Zn foil and a package film were punched to form a hole with a diameter of 12 mm at the center. Then, this Zn foil was used to assemble the symmetric cells of Zn||Zn using non-woven fabric as a separator (Fig. S9a-b). This cell was discharged/charged by a LAND CT-2001A battery tester (Fig. S9c) at a current density of 10 mA cm^{-2} for an areal capacity of 10 mAh cm^{-2}. Finally, the planar pH electrode connected with a pH meter was taken to detect the pH variation during cycles (Fig. S9d).

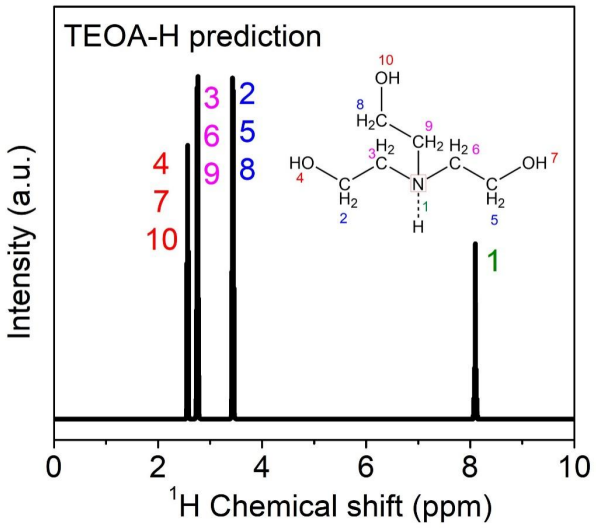

Fig. S10. The predictable ^{1}H spectrum of TEOA-H.

The N atom in original TEOA has a lone pair of electrons, and is not connected to H atom. Before the prediction of ^{1}H spectrum, an H atom is added to the N atom firstly. According to the results, if the molecule contains N-H structure, the corresponding chemical shift of the ^{1}H peak is about 8.11 ppm**.**

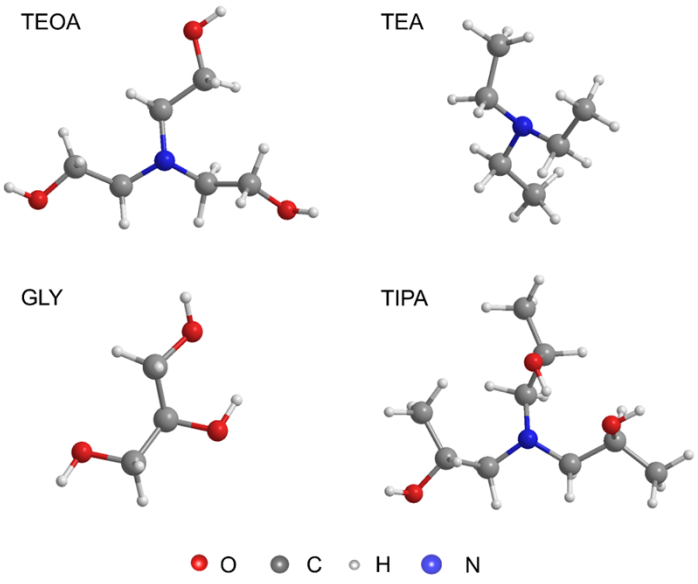

Fig. S11. The structure of TEOA, TEA, GLY and TIPA.

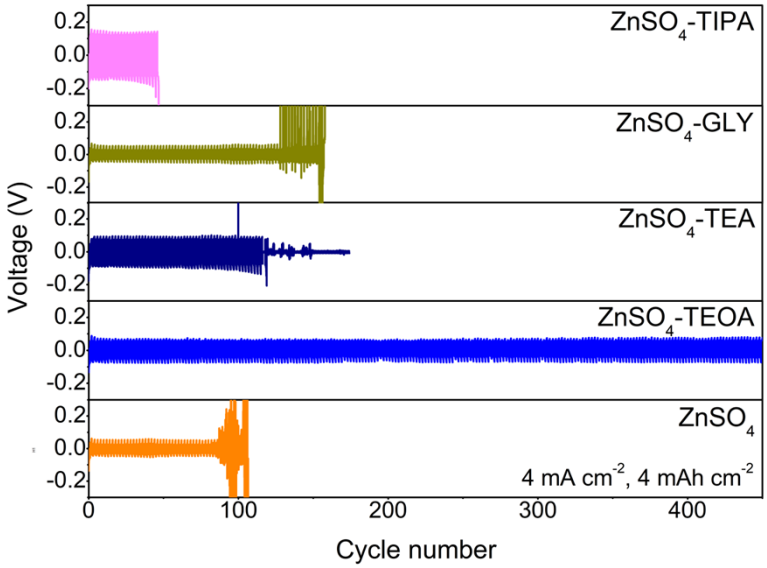

Fig. S12. Comparison of long-term cycling performance in Zn||Zn cells under 4 mA cm^{-2} and 4 mAh cm^{-2} in different electrolytes.

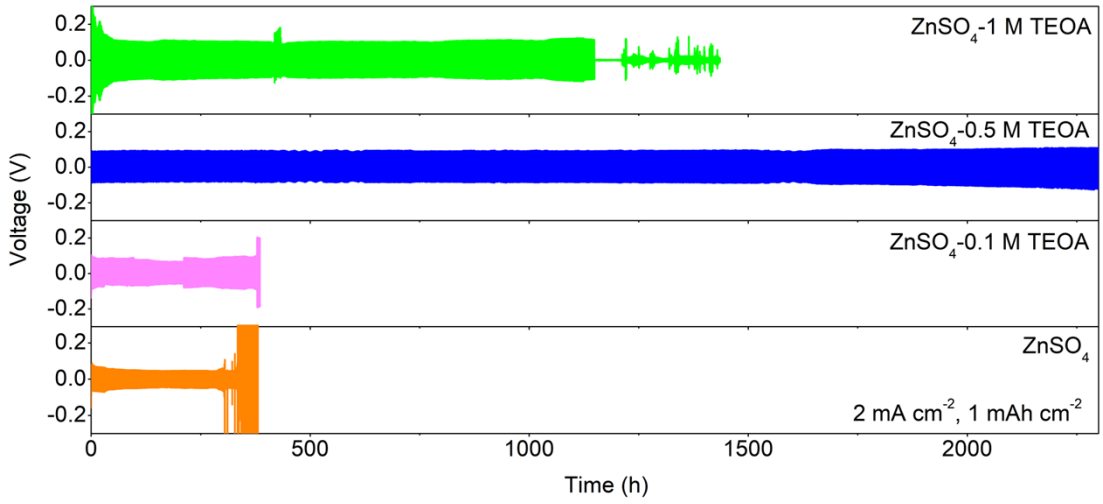

Fig. S13. Cycling performance of Zn||Zn cells in different electrolytes at 2 mA cm^{-2} and 1 mAh cm^{-2}.

Table S1. The cycling performance between this work and the previously reported based on electrolyte additives.

Electrolyte additives	Current density (mA cm^{-2})	Areal capacity (mAh cm^{-2})	Cycle number	Refs
Mu	1	1	400	4
PAA	1	1	1100	5
GLY	0.5	0.5	750	6
Z10	1	1	1000	7
TD	2	2	425	8
TEG	1	1	1000	9
SBT	1	1	525	10
DT	2	1	650	11
SMD	1	1	725	12
CTAB	2	1	2000	13
18C6	1	1	1200	14
Y^{3+}	2	2	625	15
TEOA	2	1	over 2200	This work

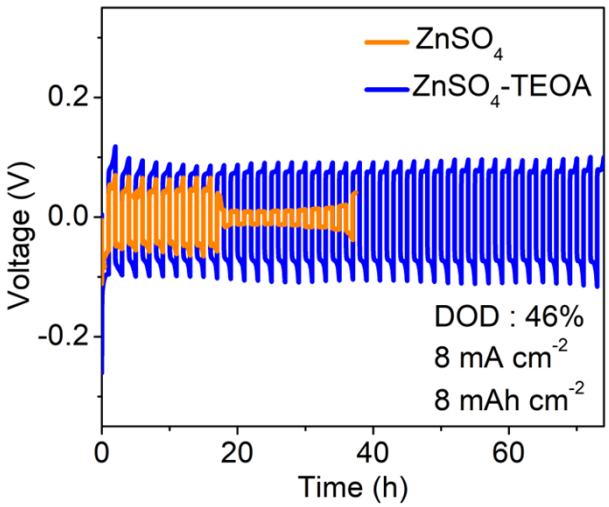

Fig. S14. Cycling performance of Zn||Zn cells under 8 mA cm^{-2} and 8 mAh cm^{-2} (DOD ~46%).

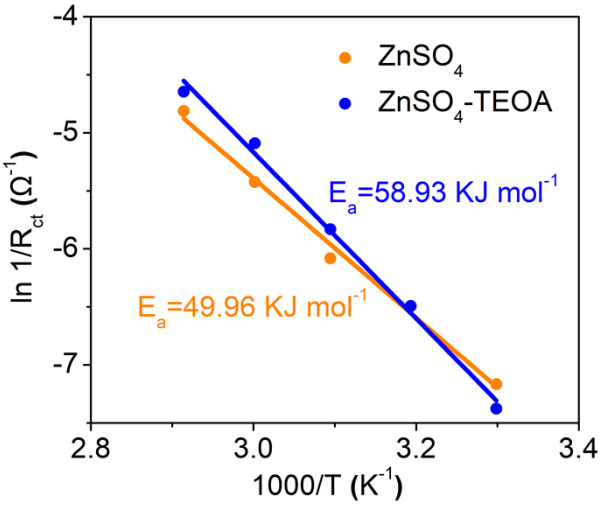

Fig. S15. The activation energies of the desolvation process of hydrated Zn^{2+} in $ZnSO_4$ and $ZnSO_4$-TEOA.

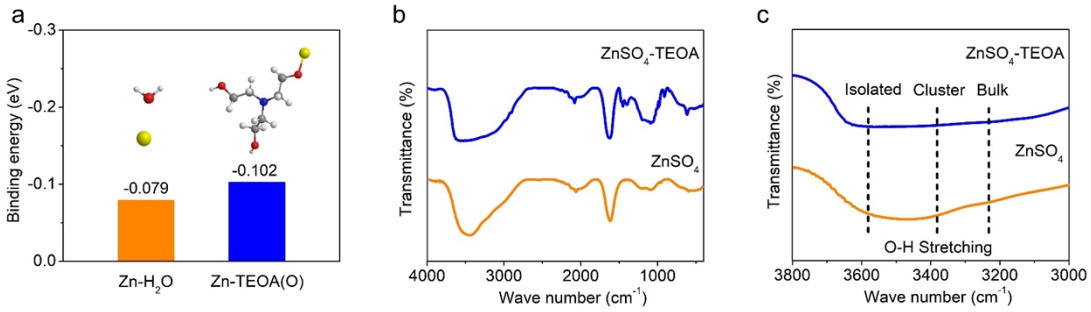

Fig. S16. (a) The binding energy of Zn^{2+} with H_2O or TEOA; (b) FT-IR spectra of different electrolytes; (c) Fitted FT-IR spectra over 3000-3800 cm^{-1}.

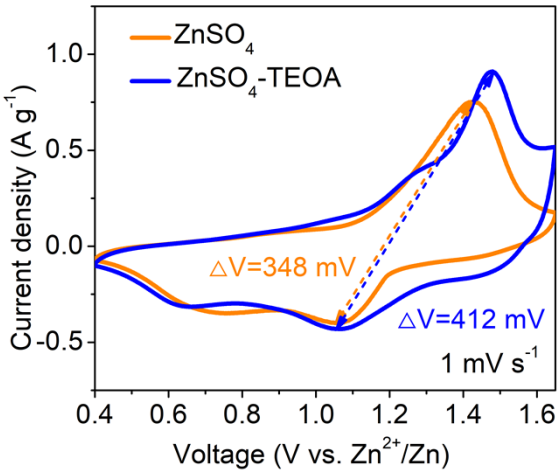

Fig. S17. CV curves of Zn||PANI full cells in $ZnSO_4$ or $ZnSO_4$-TEOA.

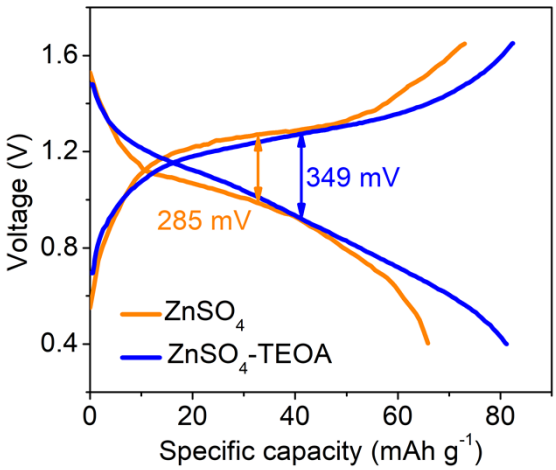

Fig. S18. Charge-discharge profiles of Zn||PANI full cells in $ZnSO_4$ or $ZnSO_4$-TEOA.

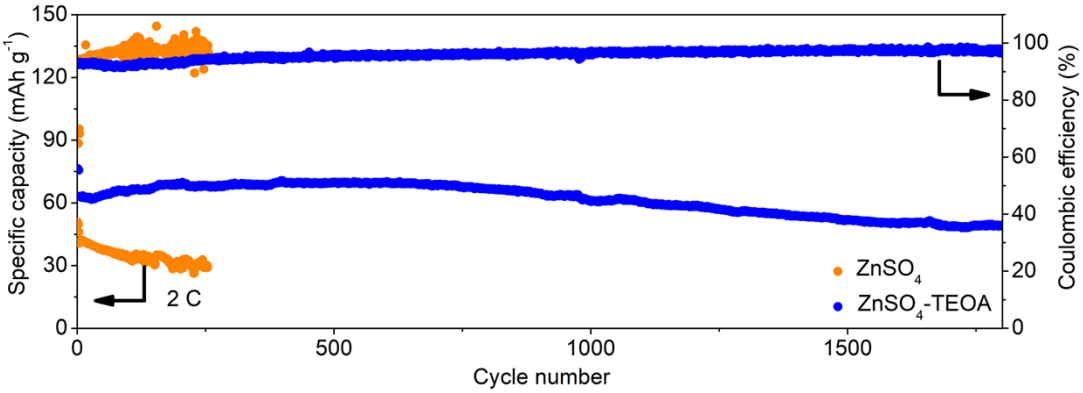

Fig. S19. Cycling performance in different electrolytes at 2 C (1 C=100 mAh g^{-1}, the full cells are activated at 0.5 C for 5 cycles).

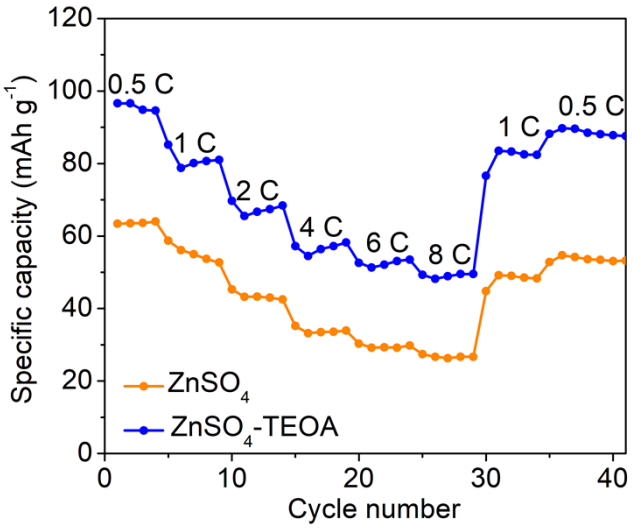

Fig. S20. Rate performances of Zn||PANI full cells in $ZnSO_4$ or $ZnSO_4$-TEOA.

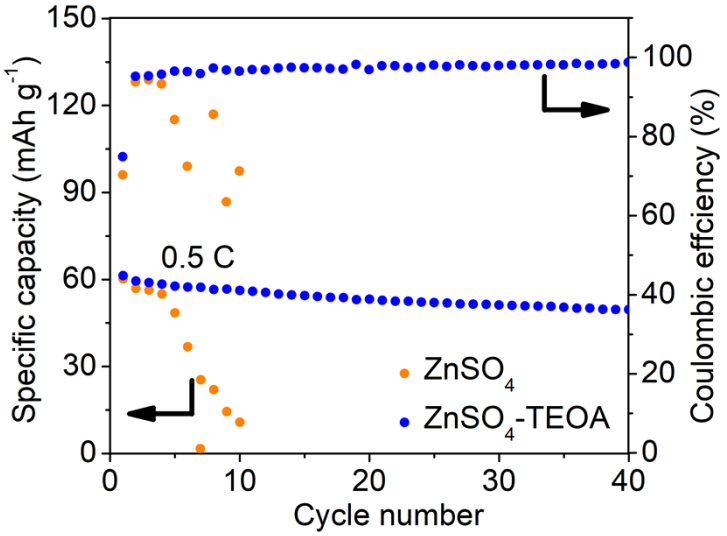

Fig. S21. Electrochemical performance of Zn||PANI (thick) full cells in different electrolytes at 0.5 C. The thickness of the anode (Zn foil) is 10 μm, the mass loading of PANI is ~ 23 mg cm^{-2} (N:P=4.2), the separator is two layers of non-woven fabric and the dosage of the electrolyte is 44.6 μL mAh^{-1}.

References

1. M. M. Voronov, A. B. Pevtsov, S. A. Yakovlev, D. A. Kurdyukov and V. G. Golubev, *Phys. Rev. B.*, 2014, **89**, 45302.
2. J. P. Perdew, K. Burke and M. Ernzerhof, *Phys. Rev. Lett.*, 1996, **77**, 3865.
3. W. Kohn and L. J. Sham, *Phys. Rev.*, 1965, **140**, A1133.
4. Y. Deng, H. Wang, M. Fan, B. Zhan, L. Zuo, C. Chen and L. Yan, *J. Am. Chem. Soc.*, 2023, **145**, 20109-20120.
5. J. Liu, W. Song, Y. Wang, S. Wang, T. Zhang, Y. Cao, S. Zhang, C. Xu, Y. Shi, J. Niu and F. Wang, *J. Mater. Chem. A.*, 2022, **10**, 20779-20786.
6. Y. Zhang, M. Zhu, K. Wu, F. Yu, G. Wang, G. Xu, M. Wu, H. Liu, S. Dou and C. Wu, *J. Mater. Chem. A.*, 2021, **9**, 4253-4261.
7. L. Tao, K. Guan, R. Yang, Z. Guo, L. Wang, L. Xu, H. Wan, J. Zhang, H. Wang, L. Hu, P. J. Dyson, M. K. Nazeeruddin and H. Wang, *Energy Storage Mater.*, 2023, **63**, 102981.
8. K. Wang, T. Qiu, L. Lin, X. Liu and X. Sun, *Energy Storage Mater.*, 2023, **54**, 366-373.
9. Y. Li, J. Cheng, D. Zhao, X. Chen, G. Sun, S. Qiao, W. Zhang and Q. Zhu, *Energy Storage Mater.*, 2023, **63**, 102997.
10. M. Qiu, P. Sun, A. Qin, G. Cui and W. Mai, *Energy Storage Mater.*, 2022, **49**, 463-470.
11. H. Peng, X. Wang, F. Yang, Z. Liu, H. Lei, S. Cui, X. Xie and G. Ma, *Chem. Eng. J.*, 2023, **474**, 145864.
12. S. Zheng, Y. Wang, B. Luo, L. Sun, G. Duan, J. Huang and Z. Ye, *Chem. Eng. J.*, 2023, **473**, 145313.
13. Z. Liu, R. Wang, Y. Gao, S. Zhang, J. Wan, J. Mao, L. Zhang, H. Li, J. Hao, G. Li, L. Zhang and C. Zhang, *Adv. Funct. Mater.*, 2023, 2308463.
14. R. Li, M. Li, Y. Chao, J. Guo, G. Xu, B. Li, Z. Liu, C. Yang and Y. Yu, *Energy Storage Mater.*, 2022, **46**, 605-612.
15. Y. Ding, X. Zhang, T. Wang, B. Lu, Z. Zeng, Y. Tang, J. Zhou and S. Liang, *Energy Storage Mater.*, 2023, **62**, 102949.